

# Analysis of real-time numerical integration methods applied to dynamic clamp experiments

Robert J Butera<sup>1</sup> and Maeve L McCarthy<sup>2</sup>

<sup>1</sup> Laboratory for Neuroengineering, Georgia Institute of Technology, Atlanta, GA 30332-0535, USA

<sup>2</sup> Department of Mathematics and Statistics, Murray State University, 6C Faculty Hall, Murray, KY 42071-3341, USA

E-mail: rbutera@ece.gatech.edu

Received 13 August 2004

Accepted for publication 8 October 2004

Published 17 November 2004

Online at [stacks.iop.org/JNE/1/187](http://stacks.iop.org/JNE/1/187)

doi:10.1088/1741-2560/1/4/001

## Abstract

Real-time systems are frequently used as an experimental tool, whereby simulated models interact in real time with neurophysiological experiments. The most demanding of these techniques is known as the dynamic clamp, where simulated ion channel conductances are artificially injected into a neuron via intracellular electrodes for measurement and stimulation. Methodologies for implementing the numerical integration of the gating variables in real time typically employ first-order numerical methods, either Euler or exponential Euler (EE). EE is often used for rapidly integrating ion channel gating variables. We find via simulation studies that for small time steps, both methods are comparable, but at larger time steps, EE performs worse than Euler. We derive error bounds for both methods, and find that the error can be characterized in terms of two ratios: time step over time constant, and voltage measurement error over the slope factor of the steady-state activation curve of the voltage-dependent gating variable. These ratios reliably bound the simulation error and yield results consistent with the simulation analysis. Our bounds quantitatively illustrate how measurement error restricts the accuracy that can be obtained by using smaller step sizes. Finally, we demonstrate that Euler can be computed with identical computational efficiency as EE.

## 1. Introduction

Numerical models of excitable cell membranes, such as neurons, routinely require the solution of gating variables. These gating variables are normalized quantities representing changes in nonlinear time- and voltage-dependent conductances of ionic currents. Approximations have been developed to speed up the computation of these gating variables, and one of the most commonly used approximations is known as ‘exponential Euler’ [1, 2].

These approximations are most often used in two situations (figure 1): (1) when laboratory experiments are coupled with real-time simulations, imposing strict temporal constraints on how rapidly the calculations for integrating the gating variables must occur [3–6], and (2) large-scale

simulations, for example of a network of neurons or a cable model of a nerve fiber, which may contain thousands of gating variables to be solved for each time step [7–12]. However, given the widespread use of this straightforward computational shortcut, a numerical analysis clearly defining the accuracy of this technique has been performed only by Victorri *et al* [13]. Their work quantifies the error in the method in terms of the change in action potential during a time step, thereby allowing for large time steps when the action potential is changing relatively slowly. We are particularly motivated to analyze this method in a different context—its use in real-time simulations interacting with experiments (also known as dynamic clamp), where there are implementation-dependent constraints on choice of step size and a measurement error associated with the experimental measurements.

In this paper we present a numerical error analysis of the exponential Euler method. The resultant error bound for a single integration time step is formulated according to the parameters of common generic forms of the gating variable equations, as well as the measurement error of a neuron's membrane potential and the size of the time step of the numerical integration. We contrast our results with those of the Euler method, which is not as widely used in these applications but is also a first-order method. We demonstrate the applicability of the method by comparing the results of highly accurate numerical simulation of a reference model with that using the exponential Euler method and calculating an error term for each time step. We conclude with a discussion of these results in the context of the accuracy and performance of dynamic clamp experiments.

### 1.1. Analysis of error in gating variables

The Hodgkin–Huxley formalism [14] represents the ionic currents in a membrane equation as a maximal conductance multiplied by one or more voltage-dependent gating variables multiplied by a voltage drive, as follows:

$$I = \bar{g} \prod_i x_i^{p_i} (V - E)$$

where  $\bar{g}$ ,  $E$  are known and the gating variables  $x_i$  are raised to integer powers  $p_i$ . The gating variables are solved according to

$$\frac{dx}{dt} = \frac{x_\infty(V)}{\tau(V)} - \frac{x}{\tau(V)} \quad (1)$$

where the functions  $x_\infty(V)$  and  $\tau(V)$  depend on the voltage  $V$ . For our particular application (figure 1(A)), the voltage  $V$  is an experimental measurement which is subject to error. Since the gating variables are normalized, they satisfy  $0 \leq X(t) \leq 1$ .

Suppose we discretize time  $0 < t_0 < t_1 < t_2 \cdots t_N = T$  with  $\Delta t = t_k - t_{k-1} = T/N$  for all  $k$ . For the gating variables and voltages, capital letters represent actual values while lower case letters represent measured values and computed values. In particular, let  $X_k$  represent the analytic solution of the differential equation using the actual voltage  $V_k$  at time  $t = t_k$ , and let  $x_k$  represent the numerical solution of the differential equation using the measured voltage  $v_k$  at time  $t = t_k$ . We define the error associated with each gating variable at time  $t = t_k$  as the difference between the actual value of the gating variable and the computed value of the gating variable

$$e_k = X_k - x_k.$$

We seek a bound on  $|e_{k+1}|$  in terms of  $|e_k|$  of the form

$$|e_{k+1}| \leq K|e_k| + L, \quad K = 1 + A\Delta t$$

because it leads to a bound of the form

$$|e_k| \leq \frac{(e^{A(\Delta t)k} - 1)L}{A\Delta t}. \quad (2)$$

See [15], lemma 1.1.

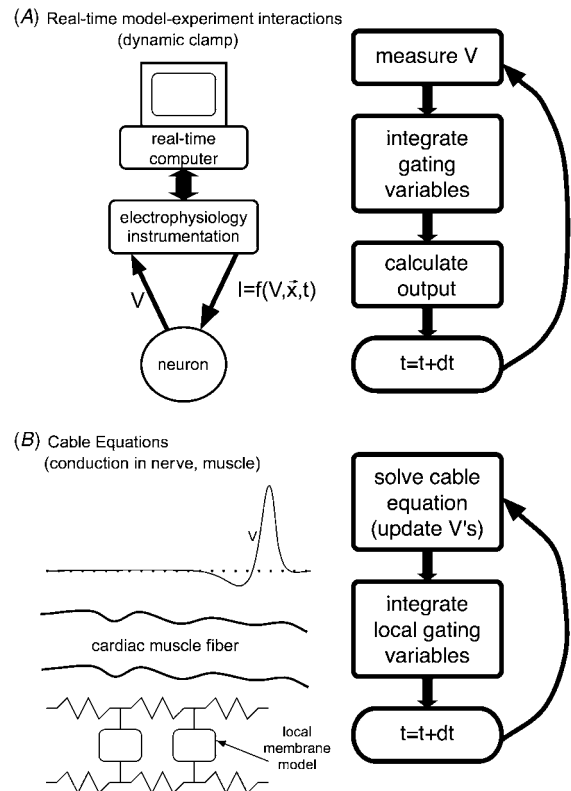


**Figure 1.** Two common applications that utilize the exponential Euler method for the integration of ionic conductance gating variables. (A) Real-time simulations coupled with experiments, where there is a fixed limit on real computation time per integrator time step. (B) Large-scale computer simulations of nervous or muscle tissue, comprising thousands of individual cellular models, where it is desired to compute each gating variable as rapidly as possible due to the sheer number of computations per time step.

We make the following assumptions:

- The experimental error in the measurement of voltage at  $t = t_k$  is bounded, i.e.,

$$|V_k - v_k| < \delta. \quad (3)$$

- The functions  $x_\infty(U)/\tau(U)$  and  $1/\tau(U)$  are Lipschitz continuous and so

$$\left| \frac{x_\infty(U)}{\tau(U)} - \frac{x_\infty(V)}{\tau(V)} \right| + \left| \frac{1}{\tau(U)} - \frac{1}{\tau(V)} \right| < \gamma|U - V|. \quad (4)$$

- The computed gating variables satisfy

$$0 \leq x_k \leq 1. \quad (5)$$

- The gating variable voltage-dependent time-constants are assumed to be positive and satisfy

$$\frac{1}{\tau(V)} \leq \frac{1}{\tau_{\min}}. \quad (6)$$

**1.1.1. Error analysis for exponential Euler method.** The exponential Euler method defines the numerical solution of (1) at time  $t_{k+1}$  as

$$x_{k+1} = x_k + (1 - e^{-\Delta t/\tau(v_k)})(x_\infty(v_k) - x_k). \quad (7)$$

The Taylor series of  $e^{-x}$  implies that

$$e^{-\Delta t/\tau(v_k)} = 1 - \frac{\Delta t}{\tau(v_k)} - \frac{e^{-\eta}(\Delta t)^2}{2\tau(v_k)^2} \quad 0 < \eta < \Delta t/\tau(v_k) \quad (8)$$

which means that

$$x_{k+1} = x_k + \left( \frac{\Delta t}{\tau(v_k)} + \frac{e^{-\eta}(\Delta t)^2}{2\tau(v_k)^2} \right) (x_\infty(v_k) - x_k). \quad (9)$$

Also by Taylor's theorem, the analytic solution of (1) satisfies

$$X_{k+1} = X_k + \Delta t \dot{X}(V_k) + \frac{(\Delta t)^2}{2} \ddot{X}(V(\xi_k)), \quad (10)$$

$$t_k < \xi_k < t_{k+1},$$

where  $\dot{X}$ ,  $\ddot{X}$  represent the first and second temporal derivatives, respectively. Using gating equation (1), this can be written as

$$X_{k+1} = X_k + \Delta t \left( \frac{x_\infty(V_k) - X_k}{\tau(V_k)} \right) + \frac{(\Delta t)^2}{2} \ddot{X}(V(\xi_k)). \quad (11)$$

Subtract (9) from (11) and group terms to obtain

$$e_{k+1} = e_k + \Delta t \left[ \left( \frac{x_\infty(V_k) - X_k}{\tau(V_k)} \right) - \left( \frac{x_\infty(v_k) - x_k}{\tau(v_k)} \right) \right] + \frac{(\Delta t)^2}{2} \left[ \ddot{X}(V(\xi_k)) - \frac{e^{-\eta}}{\tau(v_k)} \left( \frac{x_\infty(v_k) - x_k}{\tau(v_k)} \right) \right] \quad (12)$$

where  $e_k = X_k - x_k$ .

First, consider the second term of (12). By adding and subtracting  $X_k/\tau(v_k)$ , we find that

$$\left| \frac{x_\infty(V_k) - X_k}{\tau(V_k)} - \frac{x_\infty(v_k) - x_k}{\tau(v_k)} \right| \leq \left| \frac{x_\infty(V_k)}{\tau(V_k)} - \frac{x_\infty(v_k)}{\tau(v_k)} \right| + |X_k| \left| \frac{1}{\tau(v_k)} - \frac{1}{\tau(V_k)} \right| + \frac{|X_k - x_k|}{\tau(v_k)}. \quad (13)$$

From assumptions (3) through (6) it follows that

$$\left| \frac{x_\infty(V_k) - X_k}{\tau(V_k)} - \frac{x_\infty(v_k) - x_k}{\tau(v_k)} \right| \leq \gamma\delta + \frac{|e_k|}{\tau_{\min}}. \quad (14)$$

Next, consider the third term of (12). Since  $e^{-\eta} \leq e^0 = 1$ , we find that

$$\left| \ddot{X}(V(\xi_k)) - \frac{e^{-\eta}}{\tau(v_k)} \left( \frac{x_\infty(v_k) - x_k}{\tau(v_k)} \right) \right| \leq |\ddot{X}(V(\xi_k))| + \left| \frac{x_k - x_\infty(v_k)}{\tau^2(v_k)} \right|. \quad (15)$$

Under the assumption that  $dV/dt \neq 0$ , differentiation of (1) yields

$$\ddot{X}(V) = \frac{x'_\infty(V)\dot{V}}{\tau(V)} + \frac{(X - x_\infty(V))}{\tau^2(V)}(1 + \tau'(V)\dot{V}). \quad (16)$$

where  $\prime$  denotes derivatives with respect to voltage.

Since  $0 \leq X(V) \leq 1$ , and  $0 \leq x_\infty(V) \leq 1$ , it follows that  $|X(V) - x_\infty(V)| \leq 1$ . Similarly,  $|x_k - x_\infty(v_k)| \leq 1$ . Therefore

$$\left| \ddot{X}(V(\xi_k)) - \frac{e^{-\eta}}{\tau(v_k)} \left( \frac{x_\infty(v_k) - x_k}{\tau(v_k)} \right) \right| \leq \frac{|x'_\infty(V(\xi_k))\dot{V}(\xi_k)|}{\tau_{\min}} + \frac{|1 + \tau'(V(\xi_k))\dot{V}(\xi_k)|}{\tau_{\min}^2} + \frac{1}{\tau_{\min}^2}. \quad (17)$$

Using these bounds in (12), the bound for the error in the gating variables becomes

$$|e_{k+1}| \leq \left[ 1 + \frac{\Delta t}{\tau_{\min}} \right] |e_k| + \Delta t \gamma \delta + \frac{(\Delta t)^2}{2\tau_{\min}^2} (\tau_{\min} |x'_\infty(V(\xi_k))\dot{V}(\xi_k)| + |1 + \tau'(V(\xi_k))\dot{V}(\xi_k)| + 1). \quad (18)$$

Application of Gear's lemma [15] to (18) yields

$$|e_k| \leq \left( e^{\frac{k\Delta t}{\tau_{\min}}} - 1 \right) \cdot \left( \gamma\delta\tau_{\min} + \frac{\Delta t(\tau_{\min} |x'_\infty(V(\xi_k))\dot{V}(\xi_k)| + |1 + \tau'(V(\xi_k))\dot{V}(\xi_k)| + 1)}{2\tau_{\min}} \right). \quad (19)$$

Note that, if  $\dot{V}(\xi_k) = 0$ , this becomes

$$|e_k| \leq \left( e^{\frac{k\Delta t}{\tau_{\min}}} - 1 \right) \left( \gamma\delta\tau_{\min} + \frac{\Delta t}{\tau_{\min}} \right). \quad (20)$$

*1.1.2. Error analysis for the Euler method.* The Euler method defines the numerical solution of (1) at time  $t_{k+1}$  to be

$$x_{k+1} = x_k + \Delta t \left( \frac{x_\infty(v_k) - x_k}{\tau(v_k)} \right). \quad (21)$$

Subtract (21) from (11) to obtain

$$e_{k+1} = e_k + \Delta t \left( \frac{x_\infty(V_k) - X_k}{\tau(V_k)} - \frac{x_\infty(v_k) - x_k}{\tau(v_k)} \right) + \frac{(\Delta t)^2}{2} \ddot{X}(V(\xi_k)). \quad (22)$$

Using an identical analysis, we find that

$$|e_{k+1}| = |e_k| \left[ 1 + \frac{\Delta t}{\tau_{\min}} \right] + \Delta t \gamma \delta + \frac{(\Delta t)^2}{2\tau_{\min}^2} \times (\tau_{\min} |x'_\infty(V(\xi_k))\dot{V}(\xi_k)| + |1 + \tau'(V(\xi_k))\dot{V}(\xi_k)|). \quad (23)$$

Applying Gear's lemma [15], we find

$$|e_k| \leq \left( e^{\frac{k\Delta t}{\tau_{\min}}} - 1 \right) \times \left( \gamma\delta\tau_{\min} + \frac{\Delta t(\tau_{\min} |x'_\infty(V(\xi_k))\dot{V}(\xi_k)| + |1 + \tau'(V(\xi_k))\dot{V}(\xi_k)|)}{2\tau_{\min}} \right). \quad (24)$$

Note that if  $\dot{V}(\xi_k) = 0$  this becomes

$$|e_k| \leq \left( e^{\frac{k\Delta t}{\tau_{\min}}} - 1 \right) \left( \gamma\delta\tau_{\min} + \frac{\Delta t}{2\tau_{\min}} \right). \quad (25)$$

*Convergence Analysis.* Note that neither the exponential Euler nor the Euler method converges in a linear manner in the presence of measurement error. When we use  $k = N$ , we see that both methods have global error bounds of the form

$$|e_N| \leq C_1\delta + C_2\Delta t, \quad (26)$$

albeit with slightly different constants. Each method is globally linear in the absence of measurement error  $\delta$ . Locally, however, when  $k = 1$ , these methods are quadratic when  $\Delta t/\tau$  is small. It is their local behavior that is of particular interest to us because of its implications in a real-time context.

## 2. Model description

For our case study, we will consider a modified version of the model of [16], a relatively simple neuron model that can elicit periodic firing of action potentials (spiking) as well as periodic bursts of action potentials (bursting). This model is used as published, with the following modifications:

- (i) A gating variable  $m$  is used in the equation for  $I_{\text{Na}}$ , as opposed to an instantaneous function of  $V$ ; and
- (ii) The voltage-dependent time-constants are replaced by constants (not voltage-dependent) to simplify our analysis.

This model consists of four ionic currents:  $I_{\text{Na}}$  is a Hodgkin–Huxley style fast sodium current. It has a fast voltage-dependent activation gating variable ( $m$ ), and inactivation is represented by the approximation  $1 - n$  [17, 18].  $I_{\text{K}}$  is a Hodgkin–Huxley style fast potassium current. It has a moderately fast voltage-dependent activation gating variable  $n$ .  $I_{\text{NaP}}$  is a persistent sodium current with slow inactivation. It has an instantaneous function of voltage for an activation term and has a slow voltage-dependent gating variable  $h$  (not to be confused with the traditional  $h$  of the Hodgkin–Huxley equations, which was replaced by  $1 - n$  in  $I_{\text{Na}}$ ).  $I_{\text{L}}$  is a linear leakage current.

A complete set of model equations is given in the appendix. Parameters are as published except for the modifications previously noted, and for the time-constants we utilized  $\tau_m = 0.1$  ms,  $\tau_n = 10$  ms, and  $\tau_h = 10000$  ms. We utilized stimulus current values ( $I_{\text{stim}}$ ) of 14 pA and 18 pA; these two values correspond to periodic solutions of bursting and spiking, respectively. We refer to these in this manuscript as the bursting and spiking parameter values.

This bursting model was chosen for four reasons: it is relatively simple for a membrane model and thus more amenable to analysis, it is capable of a wide range of dynamic behaviors (both bursting and spiking), it contains time-constants that vary over six orders of magnitude, which will provide multiple time-scales in one model to evaluate our methods with, and these time-scales span ideal and non-ideal cases with regard to the relative values of the time-scales versus the computational time step used.

## 3. Results

Assume for each of the gating variables that  $\tau$  is independent of voltage  $V$ , i.e., it is constant, and the voltage-dependent functions are of the form

$$\begin{aligned} \tau(V) &= \tau, & x_{\infty}(V) &= (1 + e^{(V-\theta)/d})^{-1}, \\ \frac{x_{\infty}(V)}{\tau(V)} &= \frac{1}{(1 + e^{(V-\theta)/d})\tau} \\ x'_{\infty}(V) &= \frac{-e^{(V-\theta)/d}}{d(1 + e^{(V-\theta)/d})^2} = \frac{-1}{d(e^{-(V-\theta)/2d} + e^{(V-\theta)/2d})^2} \\ &= \frac{-1}{4d \cosh^2((V - \theta)/d)}. \end{aligned}$$

Apply the mean value theorem

$$\left| \frac{x_{\infty}(U)}{\tau(U)} - \frac{x_{\infty}(V)}{\tau(V)} \right| = \left| \left( \frac{x_{\infty}(W)}{\tau(W)} \right)' \right| |U - V| \leq \frac{|U - V|}{4\tau|d|} \quad (27)$$

for some  $W$  in  $(U, V)$ :

$$\left| \frac{1}{\tau(U)} - \frac{1}{\tau(V)} \right| = \left| \frac{1}{\tau} - \frac{1}{\tau} \right| = 0.$$

Thus we can identify

$$\gamma = \frac{1}{4\tau|d|}, \quad \tau_{\min} = \tau, \quad |x'_{\infty}| \leq \frac{1}{4|d|}, \quad \tau' = 0.$$

Assuming in both cases that  $\dot{V}(\xi_k) = 0$ , we are most interested in one-step (local) error bounds where  $k = 1$ . This results in the following bounds for exponential Euler and Euler, respectively:

$$|e|_{\text{exEuler}} \leq (e^{\frac{\Delta t}{\tau}} - 1) \left( \frac{\delta}{4|d|} + \frac{\Delta t}{\tau} \right) \quad (28)$$

$$|e|_{\text{Euler}} \leq (e^{\frac{\Delta t}{\tau}} - 1) \left( \frac{\delta}{4|d|} + \frac{\Delta t}{2\tau} \right). \quad (29)$$

The values used for  $\tau$  and  $d$  are obtained directly from the model parameters. The measurement error,  $\delta$ , represents two sources of uncertainty. First is the actual error in the measurement of membrane voltage during an experiment; for these reference simulations using a deterministic model, we can assume that this error is zero. However, a second source of measurement error is the fact that both of these numerical methods are explicit, and the dynamical equations for the gating variables are dependent on  $V$  and assume that the temporal change in  $V$  is insignificant over a single time step. In fact, this assumption is implicit in the development of the exponential Euler method. Figure 2 illustrates  $|\Delta V|$  versus time for repetitively firing action potentials with a time-step of 0.1 ms (corresponding to a computational rate of 10 kHz, a commonly used rate in dynamic clamp experiments). A bound of 0.7 mV (dashed line) sufficiently bounds  $|\Delta V|$  for the entire action potential cycle except during the rapid upstroke of the action potential. While this bound could be made larger (and result in a larger value for  $\delta$ ), it will be shown later that choosing  $\delta = 0.7$  mV provides values of  $\delta$  that yield error bounds that are sufficient, and a more liberable bound is both unnecessary and less informative.

### 3.1. Local error analysis

For our reference simulations, we performed a local or one-step error analysis. This consisted of performing a highly accurate numerical simulations for both the bursting and spiking models. These simulations used the CVODE numerical integration method [19] for stiff systems. For these reference simulations, the absolute and relative error tolerances were set to  $10^{-5}$  and output was recorded every 0.1 ms (although the adaptive step size used may be significantly small or larger than this). These and all subsequent simulations were implemented using the dynamical systems environment XPPAUT [20] unless otherwise noted.

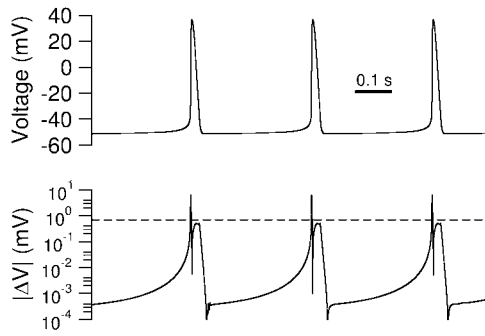


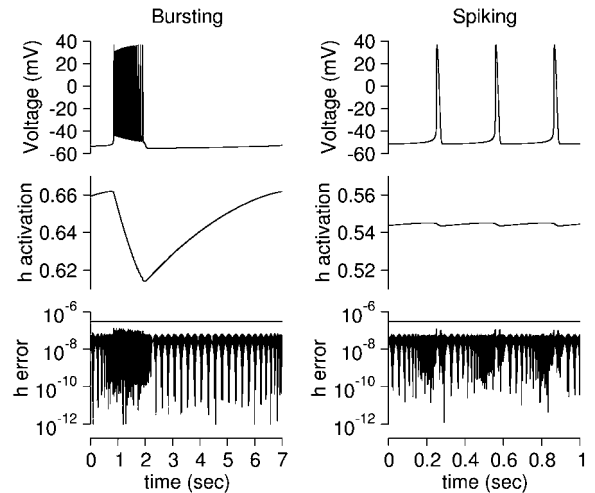
**Figure 2.**  $V$  and  $|\Delta V|$  versus time for a time step of 0.1 ms for stable repetitively firing action potentials using the reference model with  $I_{\text{app}} = 18$  pA. The y-axis is a log scale. Dashed line is for  $|\Delta V| = 0.7$  mV.

Recall that a local error is the error after one time step of integration. This form of error is especially appropriate for analysis of real-time experimental control systems (figure 1(A)), where the integration of the gating variables is dependent on a new measurement made during each computational cycle. We utilized a step-size ( $\Delta t$ ) of 0.1 ms for two reasons: this step size corresponds to a periodic computational rate of 10 kHz, commonly used in dynamical clamp experiments, and this step size will highlight the relative effects of  $\tau$  on the accurate computation of the trajectory of the gating variables.

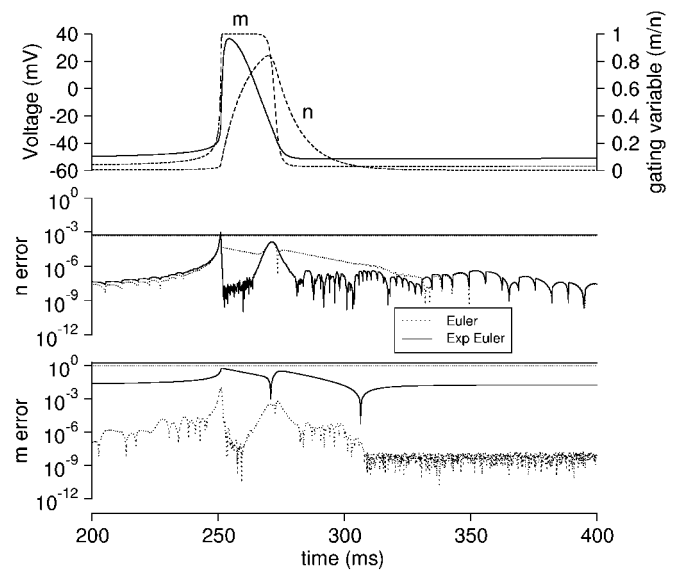
Local error was calculated by using the values of *each* state vector at each timepoint in the reference simulations as an initial condition, and then performing one step of either Euler or exponential Euler integration. The results of this integration were then subtracted from the next state vector in the reference simulation to obtain an error term. These one-step errors were calculated for parameter values corresponding to bursting and spiking dynamics, and these errors were also compared to the error bound computed for the Euler and exponential Euler integration of the gating variables according to equations (28) and (29). To compute these error bounds,  $\Delta t$  was 0.1 ms,  $\delta$  was 0.7 mV (figure 2), and value for  $k$  and  $\tau$  were obtained from the reference model.

Figure 3 illustrates bursting and spiking dynamics, and corresponding changes in membrane potential ( $V$ ) and the gating variable  $h$ . This gating variable has an extremely slow time constant. During spiking, changes in  $h$  are almost negligible. In both dynamic modes, the one-step error for both Euler and exponential Euler are indistinguishable on the graph. The predicted error bounds are also nearly identical and the one-step error in  $h$  is well below these bounds. This is hardly surprising, given how slow the time constant of  $h$  is related to step size. For this reason, the remainder of our analysis focuses on the dynamics of the faster gating variables  $m$  and  $n$  that underlie spiking.

The time courses of the faster gating variables  $m$  ( $\tau = 0.1$  ms) and  $n$  ( $\tau = 10$  ms) during the repetitive firing of an action potential (spiking) are illustrated in figure 4. The remaining panels of figure 4 illustrate the one-step error and predicted error bounds for both gating variables using both numerical methods. When examining the dynamics of  $n$ , the



**Figure 3.** Comparison of bursting and spiking dynamics. Simulations shown for one or more periods of oscillation of the model in parameter regimes corresponding to bursting (left) and spiking (right). Panels illustrate (top to bottom) membrane potential, time course of  $h$  gating variable, and one-step error of  $h$  gating variable (solid—Euler, dashed—exponential Euler). The one-step errors are indistinguishable in this case. Horizontal lines in bottom panel illustrated predicted error bound (solid and dotted, indistinguishable).



**Figure 4.** Spiking dynamics and one-step error of fast gating variables. Same simulation as the right panel of figure 3, zoomed on a 200 ms window about the first spike. Top panel illustrates changes in  $V$  (solid line) and gating variables  $m$  and  $n$  (dashed lines). Middle and bottom panels illustrate one-step error in  $n$  and  $m$ , respectively. Each of the error panels plots the error for both the Euler and exponential Euler method, and horizontal lines indicate predicted error bounds.

error bounds were similar. The exponential Euler method has less error than the Euler method at the maximal and minimal points of the action potential, since this is where the critical assumption of this method,  $\dot{V} = 0$ , is most valid. More significantly, however, is the fact that the peak error for both methods was similar and occurred during the maximal changes of  $V$  on the upstroke and downstroke of the action potential. The one-step error for  $m$  was quite different when comparing

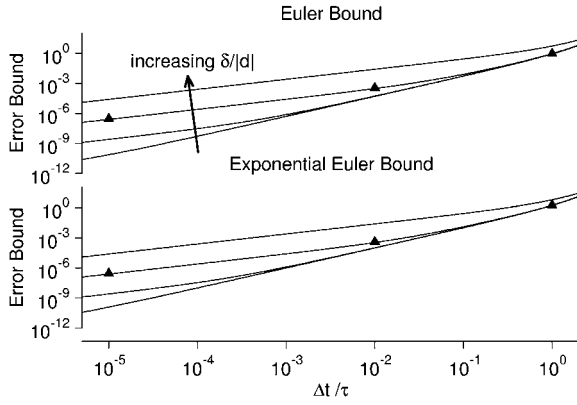


**Figure 5.** Magnitude of predicted error for Euler and exponential Euler as a function of the ratios  $\delta/|d|$  and  $\Delta t/\tau$ . Curves are parametrized by  $\delta/|d| = 10^{-5}, 10^{-3}, 10^{-1}$  and 10. Triangles represent corresponding error bounds using model parameters for  $h, n$  and  $m$  (left to right).

the two methods. It should be noted that the dynamics of  $m$  are a ‘worst case’ scenario:  $\tau$  is 0.1 ms, the same as the computational step size. In this case, the one-step error using the exponential Euler method was significantly worse than that using the Euler method. For both  $m$  and  $n$ , the predicted error bounds did a reasonable job identifying the limits of the one-step error.

### 3.2. Relationship between measurement error and time step

Examining equations (28) and (29), it is clear that the error bound scales with two ratios:  $\delta/|d|$  and  $\Delta t/\tau$ . The first is a ratio of the voltage-measurement error divided by the slope factor of the gating variable in question, the second is the ratio of the time step to the time constant of the gating variable. Figure 5 illustrates a plot of these error bounds as a function of  $\Delta t/\tau$  for different values of  $\delta/|d|$ . Clearly two slopes are evident: one when  $\Delta t/\tau < \delta/|d|$ , and another when  $\Delta t/\tau > \delta/|d|$ . It is apparent that when  $\Delta t/\tau$  is large relative to  $\delta/|d|$ , no amount of improvement in measurement error can improve the error bound due to the numerical inaccuracies caused by a relatively large time step. Conversely, if  $\Delta t/\tau$  is small relative to  $\delta/|d|$ , an order of magnitude improvement in  $\delta$  results in a similar order of magnitude in the error bound. In practice, the voltage-measurement error  $\delta$  contributes more significantly to the error in the computation than the numerical error associated with the step size  $\Delta t$ .

A natural question to consider is the following: in the presence of experimental error  $\delta$ , how small does the step size  $\Delta t$  need to be in order to guarantee that the error in the gating variable is at an acceptable level? This can be computed by bounding the right hand sides of equations (28) and (29) by an acceptable error level  $A$  and solving the resulting nonlinear inequalities. Note that when  $\Delta t/\tau \ll 1$ , we can use  $e^{\frac{\Delta t}{\tau}} - 1 \approx \Delta t/\tau$  and the inequalities become

$$\frac{\Delta t}{\tau} \left( \frac{\delta}{4|d|} + \frac{\Delta t}{\tau} \right) \leq A_{\text{exEuler}}$$

$$\frac{\Delta t}{\tau} \left( \frac{\delta}{4|d|} + \frac{\Delta t}{2\tau} \right) \leq A_{\text{Euler}}$$

giving upper bounds of

$$\Delta t \leq \frac{\tau}{8|d|} \left( -\delta + \sqrt{\delta^2 + 64|d|A_{\text{exEuler}}} \right)$$

and

$$\Delta t \leq \frac{\tau}{16|d|} \left( -\delta + \sqrt{\delta^2 + 32|d|A_{\text{Euler}}} \right)$$

for our step size  $\Delta t$ .

Over more than one integration step, local errors can accumulate and contribute to a global error of the form given by equations (20) and (25). For our simulation, the global error has the form

$$|e|_{\text{exEuler}} \leq \left( e^{\frac{N\Delta t}{\tau}} - 1 \right) \left( \frac{\delta}{4|d|} + \frac{\Delta t}{\tau} \right)$$

$$|e|_{\text{Euler}} \leq \left( e^{\frac{N\Delta t}{\tau}} - 1 \right) \left( \frac{\delta}{4|d|} + \frac{\Delta t}{2\tau} \right)$$

where  $N$  is the number of time steps taken. Since  $N\Delta t = T$ , if we choose  $\Delta t$  so that

$$\left( e^{\frac{T}{\tau}} - 1 \right) \left( \frac{\delta}{4|d|} + \frac{\Delta t}{\tau} \right) \leq A_{\text{exEuler}}$$

$$\left( e^{\frac{T}{\tau}} - 1 \right) \left( \frac{\delta}{4|d|} + \frac{\Delta t}{2\tau} \right) \leq A_{\text{Euler}}$$

we can guarantee that the global error is below a certain level for a dynamic clamp experiment that lasts  $T$  s. However, we believe that this consideration of global error is unnecessary and/or impractical for several reasons. First, the global error is absolute, and accumulates every time step without bound. However, the neural systems studied by a dynamic clamp are typically oscillatory (resulting in positive and negative error) and the differential equations formulating the gating variables typically bound the dynamics between 0 and 1. Both of these factors make it unlikely in practice that error would grow without bound. Second, we have found that even in worst-case scenarios, the global error at a given time step is typically an order of magnitude or more larger than the actual computed error. Third, even if global error was a significant concern, the process outlined above using physiological constants would likely result in values for  $\Delta t$  that are significantly smaller than can be practically implemented by real-time systems.

### 3.3. Methods for real-time implementation

It has previously been noted by several authors [4, 5] that a primary motivation of using the exponential Euler method in real-time methods is its rapid calculation. When modeling a voltage-dependent gating variable  $x$  with a voltage-dependent time constant and activation curve, through the use of lookup tables as a function of the digitized measured voltage it is possible to reduce the integration of a gating variable to two table lookups and a single multiple and single add operation:

$$x^* = F_1(V) \quad (30)$$

$$x+ = F_2(V) \quad (31)$$

where  $F_1(V)$  and  $F_2(V)$  are functions implemented by voltage-dependent lookup tables. It is possible to implement

**Table 1.** Table lookup implementation for Euler and exponential Euler methods when using a one-step multiply-add update.

	$F_1(V)$	$F_2(V)$
Euler	$1 - \frac{\Delta t}{\tau(V)}$	$\frac{\Delta t}{\tau(V)} x_\infty(V)$
Exponential Euler	$e^{-\frac{\Delta t}{\tau(V)}}$	$x_\infty(V) (1 - e^{-\frac{\Delta t}{\tau(V)}})$

both Euler and exponential Euler in this way, thus speed of implementation is no rationale for choosing one method over another. Table 1 lists the functional implementation of  $F_1(V)$  and  $F_2(V)$  for both methods.

#### 4. Discussion

In this paper we have developed a local error analysis of the Euler and exponential Euler methods applied to the numerical integration of voltage-dependent gating variables. Our approach was motivated by the ‘dynamic clamp’ application, where the voltages driving the gating variables are subject to measurement error. We showed that both the Euler and exponential Euler methods perform comparably when  $\Delta t < \tau$ . In practice, investigators prefer that  $\Delta t/\tau$  is 0.1 or smaller to maintain numerical accuracy in real-time simulations. However, sometimes investigators are forced to violate this practice due to the computational complexity of their real-time model. In these non-ideal cases, the Euler method performed better. The conclusions of our numerical tests are consistent with the error bounds established in this paper. When  $\Delta t/\tau$  is small, the error bound is similar for both methods, but when  $\Delta t/\tau$  is large, exponential Euler has a lower local error bound.

We further derived analytical formulae using the error bounds whereby, for a known voltage measurement error  $\delta$  and desired one-step integration accuracy  $A$ , one can compute the time step necessary to achieve the desired accuracy. This is of utility as a guide to choosing the computational cycle duration for a real-time system interacting with neurophysiological experiments, and we intend to incorporate it into the next version of our own real-time system for electrophysiological experiments, MRCI [6], available online at <http://www.neuro.gatech.edu/mrci/>.

Most approaches to numerical analysis of differential equations consider the order of a method from a global perspective. If one makes the assumption that  $\Delta t \ll \tau$ , the exponential Euler method reduces to the Euler method. Such observations may lead to the impression that exponential Euler is more accurate. However, as our local error bounds illustrate, such assumptions of improved accuracy are misleading.

To our knowledge, this study is the first to consider the numerical methods used to integrate gating variables in real time, considering the perspectives of voltage measurement error and the constraints upon  $\Delta t$ . Unlike traditional model simulations, with real-time systems it is not practical to make  $\Delta t$  smaller and simply wait longer for the simulation result. However, much work still needs to be done to investigate the question of to what extent, given voltage measurement error, it is useful to implement higher-order numerical methods in a real-time system interacting with experiments. The improved

accuracy of such methods would have to be evaluated not only in light of voltage measurement error, but also to consider that the use of higher-order methods requires greater computational resources and thus increases the minimal value of  $\Delta t$  that is feasible.

#### Acknowledgments

This work was supported by a Research Opportunity Award supplement from the National Science Foundation (DBI-9987074) and the James S McDonnell Foundation. The Petit Institute for Bioengineering and Biosciences, the School of Electrical and Computer Engineering, and the Wallace H Coulter Department of Biomedical Engineering at Georgia Tech and Emory University contributed laboratory space and/or resources used to conduct this research.

#### Appendix. Model equations

The reference model for performance analysis is a Hodgkin–Huxley [14] style model. It is a minimal model for oscillatory bursting [16] exhibited by respiratory pacemaker neurons in the pre-Bötzinger complex of the mammalian ventrolateral medulla [21, 22]. For this particular paper, time constants were simplified to be non-voltage dependent, and the activation of  $I_{Na}$  has been modified to be noninstantaneous and activated by the gating variable  $m$ . Not counting membrane voltage (which is integrated by the model neuron), this model consists of three state variables ( $m, n, h$ ) and four ionic currents. The model equations are described as follows:

$$\dot{m} = (m_\infty(V) - m)/\tau_m \quad (32)$$

$$\dot{n} = (n_\infty(V) - n)/\tau_n \quad (33)$$

$$\dot{h} = (h_\infty(V) - h)/\tau_h \quad (34)$$

$$I_K = \bar{g}_K n^4 (V - E_K) \quad (35)$$

$$I_{Na} = \bar{g}_{Na} m^3 (V - E_{Na}) \quad (36)$$

$$I_{NaPh} = \bar{g}_{NaPh} p_\infty(V) h (V - E_{Na}) \quad (37)$$

$$I_L = \bar{g}_L (V - E_L) \quad (38)$$

$$I_m = I_{Na} + I_K + I_{NaPh} + I_L - I_{stim} \quad (39)$$

where  $V$  is the measured membrane potential and  $I_{stim}$  is an applied stimulus current parameter.  $I_m$  is the total transmembrane current. The voltage-dependent steady-state activation functions ( $n_\infty(V), h_\infty(V), m_\infty(V), p_\infty(V)$ ) are of the form  $x_\infty(V) = 1/(1 + \exp((V - \theta_x)/d_x))$ .

Gating variable parameters are specified in table 2. Additional parameters are as follows:  $\bar{g}_{Na} = 28$  nS,  $\bar{g}_K = 11.2$  nS,  $\bar{g}_{NaPh} = 2.8$  nS,  $\bar{g}_L = 2.8$  nS,  $E_{Na} = 50$  mV,  $E_K = -85$  mV,  $E_L = -65$  mV. For reference simulations

**Table 2.** Parameters for gating variable differential equations.

Variable $x$	$\theta_x$ (mV)	$d_x$ (mV)	$\tau_x$ (ms)
$m$	-34	-5	0.1
$n$	-29	-4	10.0
$h$	-48	6	10 000
$p$	-40	-6	NA

where voltage was integrated along with the gating variables,  $\frac{dV}{dt} = -\frac{I_m}{C_m}$ , where  $C_m = 28$  pF.

## References

- [1] Moore J W and Ramon F 1974 On numerical integration of the Hodgkin and Huxley equations for a membrane action potential *J. Theor. Biol.* **45** 249–73
- [2] Rush S and Larsen H 1978 A practical algorithm for solving dynamic membrane equations *IEEE Trans. Biomed. Eng.* **36** 389–92
- [3] Sharp A A, O'Neil M B, Abbott L F and Marder E 1993 Dynamic clamp: computer-generated conductances in real neurons *J. Neurophys.* **69** 992–5
- [4] Butera R J, Wilson C G, DelNegro C A and Smith J C 2001 A methodology for achieving high-speed rates for artificial conductance injection in electrically excitable cells *IEEE Trans. Biomed. Eng.* **48** 1460–70
- [5] Dorval A D, Christini D J and White J A 2001 Real-time Linux dynamic clamp: A fast and flexible way to construct virtual ion channels in living cells *Ann. Biomed. Eng.* **29** 897–907
- [6] Raikov I, Preyer A and Butera R J 2004 MRCl: A flexible real-time dynamic clamp system for electrophysiology experiments *J. Neurosci. Methods* **132** 109–23
- [7] Ten Tusscher K H and Panfilov A V 2003 Reentry in heterogeneous cardiac tissue described by the Luo-Rudy ventricular action potential model *Am. J. Physiol.* **284** H542–H548
- [8] Qu Z and Garfinkel A 1999 An advanced algorithm for solving partial differential equation in cardiac conduction *IEEE Trans. Biomed. Eng.* **46** 1166–88
- [9] Nygren A and Halter J A 1999 A general approach to modeling conduction and concentration dynamics in excitable cells of concentric cylindrical geometry *J. Theor. Biol.* **199** 329–58
- [10] Pollard A E and Barr R C 1991 Computer simulations of activation in an anatomically based model of the human ventricular conduction system *IEEE Trans. Biomed. Eng.* **38** 982–96
- [11] Halter J A and Clark J W 1991 A distributed parameter model of the myelinated nerve fiber *J. Theor. Biol.* **7** 345–82
- [12] Murphey C R, Clark J W, Giles W R, Rasmusson R L, Halter J A, Hicks K and Hoyt B 1991 Conduction in bullfrog atrial strands: simulations of the role of disc and extracellular resistance *Math. Biosci.* **106** 39–84
- [13] Victorri B, Vinet A, Roberge F A and Drouhard J P 1985 Numerical integration in the reconstruction of cardiac action potentials using the Hodgkin Huxley model *Computers and Biomed. Res.* **18** 10–23
- [14] Hodgkin A L and Huxley A F 1952 A quantitative description of membrane current and its application to conduction and excitation in nerve *J. Physiol. (Lond.)* **116** 500–44
- [15] Gear C W (ed) 1971 *Numerical Initial Value Problems in Ordinary Differential Equations* (Englewood Cliffs, NJ: Prentice-Hall)
- [16] Butera R J, Rinzel J and Smith J C 1999 Models of respiratory rhythm generation in the pre-Bötzinger complex: I. Bursting pacemaker neurons *J. Neurophysiol.* **82** 382–97
- [17] Krinsky V I and Kokoz Y M 1973 Analysis of the equations of excitable membranes. I. Reduction of the Hodgkin–Huxley equations to a second order system *Biofizika* **18** 506–11
- [18] Rinzel J 1985 Excitation dynamics: insight from simplified membrane models *Fed. Proc.* **44** 2944–6
- [19] Cohen S D and Hindmarsh A C 1996 CVODE: A stiff/nonstiff ODE solver in C *Comput. Phys.* **10** 138–43
- [20] Ermentrout G B 2002 *Simulating, Analyzing, and Animating Dynamical Systems: A Guide to Xppaut for Researchers and Students* (Providence, RI: Society for Industrial and Applied Mathematics)
- [21] Smith J C, Ellenberger H H, Ballanyi K, Richter D W and Feldman J L 1991 Pre-Bötzinger complex: a brainstem region that may generate respiratory rhythm in mammals *Science* **254** 726–9
- [22] Koshiya N and Smith J C 1999 Neuronal pacemaker for breathing visualized *in vitro Nature* **400** 360–3